MASTER COPY KEEP THIS COPY FOR REPRODUCTION PURPOSES

REPORT DOCUMENTATION PAGE

Form Approved
OMB No. 0704-0188

1. AGENCY USE ONLY (Leave blank)	2. REPORT DATE	3. REPORT TYPE AND DATES COVERED
	27 September 1995	Technical

4. TITLE AND SUBTITLE

Pore Structure Model for Water and Contaminant Transport in Soil

5. FUNDING NUMBERS

DAAH04-94-C-0075

6. AUTHOR(S)

Girard A. Simons

7. PERFORMING ORGANIZATION NAME(S) AND ADDRESS(ES)

Simons Research Associates
3 Juniper Road
Lynnfield, MA 01940-2416

8. PERFORMING ORGANIZATION REPORT NUMBER

9. SPONSORING/MONITORING AGENCY NAME(S) AND ADDRESS(ES)

U.S. Army Research Office
P.O. Box 12211
Research Triangle Park, NC 27709-2211

10. SPONSORING/MONITORING AGENCY REPORT NUMBER

ARO 32900.5-GS-S

11. SUPPLEMENTARY NOTES

The views, opinions and/or findings contained in this report are those of the author(s) and should not be construed as an official Department of the Army position, policy, or decision, unless so designated by other documentation.

12a. DISTRIBUTION/AVAILABILITY STATEMENT

Approved for public release; distribution unlimited.

12b. DISTRIBUTION CODE

13. ABSTRACT *(Maximum 200 words)*

The "pore tree" model of pore structure (Simons and Finson, 1979; Simons, 1982) was developed for catalyst and sorbent grains to allow coupled reactions and diffusion into and out of immobile porous media in the absence of convection through the media. The pore tree model is extended herein to describe the permeable (mobile) pore structure which characterizes the subsurface transport of gas and water in soil, the dispersion of contaminants, and in-situ remediation. The interconnectivity of the pore structure is obtained via a statistical determination of the "branches" that are common to several trees to allow convection and diffusion through the large scale (mobile) structure in addition to diffusion and reactions in the small scale (immobile) structure. The extended pore tree model has explained the measurement errors in the permeability of soil due to the measurement scale size (Shouse et. al., 1994) and has successfully predicted the bulk gaseous diffusivity in partially saturated soil (Washington et. al., 1994) as a function of a saturation scale size. The theory also depicts a permeable sub-range in which small scale convection bridges the flow between the bulk convection and the small scale diffusion.

14. SUBJECT TERMS	15. NUMBER OF PAGES
DTIC QUALITY INSPECTED 5 Pore Structure, Interconnectivity, Permeability, Bulk Diffusivity	21
	16. PRICE CODE

17. SECURITY CLASSIFICATION OF REPORT	18. SECURITY CLASSIFICATION OF THIS PAGE	19. SECURITY CLASSIFICATION OF ABSTRACT	20. LIMITATION OF ABSTRACT
UNCLASSIFIED	UNCLASSIFIED	UNCLASSIFIED	UL

NSN 7540-01-280-5500

Standard Form 298 (Rev. 2-89)
Prescribed by ANSI Std. Z39-18
298-102

PORE STRUCTURE MODEL FOR WATER AND CONTAMINANT TRANSPORT IN SOIL

Interim Report

For The Period 28 September 1994 To 27 September 1995

Girard A. Simons

27 September 1995

U.S. Army Research Office

Contract/Grant Number DAAH04-94-C-0075

Simons Research Associates
3 Juniper Road
Lynnfield, MA 01940-2416

Approved For Public Release;
Distribution Unlimited

THE VIEWS, OPINIONS, AND/OR FINDINGS CONTAINED IN THIS REPORT ARE THOSE OF THE AUTHOR AND SHOULD NOT BE CONSTRUED AS AN OFFICIAL DEPARTMENT OF THE ARMY POSITION, POLICY, OR DECISION, UNLESS SO DESIGNATED BY OTHER DOCUMENTATION.

TABLE OF CONTENTS

I. INTRODUCTION

To properly describe coupled chemical reactions and gaseous diffusion in porous sorbent and catalyst grains, the "pore tree" was introduced by Simons and Finson (1979) and Simons (1982). The pore tree represents an isolated sub-structure, allowing diffusion into and out of the porous media without permitting transport through the media. This pore structure was developed via analogy to the kinetic theory of gases with the pore length analogous to the mean free path. Under the assumption that the pore aspect ratio (pore length to radius) is a constant, a pore size distribution was obtained that has been confirmed for coal, coal char, sorbents, catalysts and kidney stones from both men and women. The pore tree was statistically derived from the pore size distribution and allows the orderly migration of a reactant gas from the large pores to the small pores (Fig. 1). A detailed description of the pore tree and the coupled transport and chemistry is given by Simons (1982, 1983a). The spatially dependent transport/reaction equations are solved for a single pore tree and then the total contribution of all trees (of all sizes) in the system is obtained by summing the contribution of each tree that reaches the exterior of the system. This is distinct from the "bulk" transport approach in which the transport equation for a single pore is integrated over all pores at a fixed point in space before integrating spatially. The "bulk" transport approach is invalid if the spatial gradients in the transport equations are implicit functions of pore size. One example of this implicit pore size dependence is that of the heterogeneous reactions within porous catalysts and sorbents for which the pore tree structure/transport model was developed. A second example is that of coupled diffusion and remediation reactions in the immobile region of soil.

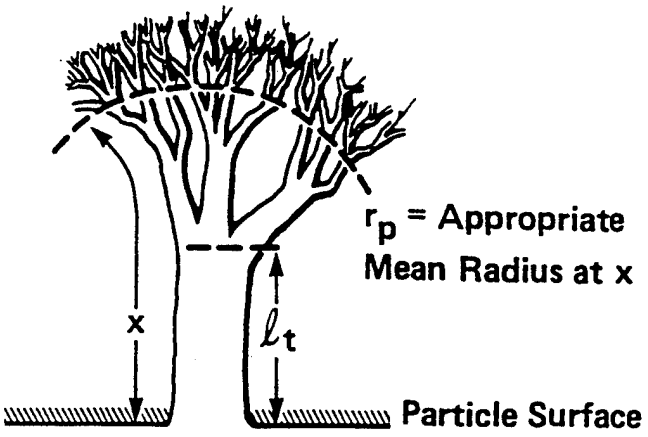

Figure 1. The Pore Tree

In order to describe the subsurface transport of gas and water in soil, the dispersion of contaminants, and in-situ remediation of contaminated sites, the pore tree is extended herein to simulate permeability and bulk transport. The random nature of the pore structure, which formed the basis of the statistical derivation of the pore tree, is applied to porous soil and sand. The interconnectivity of the pore structure is obtained via a statistical determination of the "branches" that are common to several trees to allow convection and diffusion through the large scale (mobile) structure in addition to diffusion and coupled reactions in the small scale (immobile) structure. The extended pore tree model has been used to explain the measurement errors in the permeability of soil due to the measurement scale size (Shouse et. al., 1994) and has successfully predicted the bulk gaseous diffusivity in partially saturated soil (Washington et. al., 1994) as a function of a saturation scale size. The theory also depicts a permeable sub-range in which small scale convection bridges the flow between the bulk convection and the small scale diffusion. The model provides an analytic description of a pore structure for soil upon which transport and coupled chemical reactions may be accurately superimposed.

II. ISOLATED PORE TREE: THE STRUCTURE

Following the pore structure theory of Simons and Finson (1979) and Simons (1982), consider a spherical porous particle of radius a, containing pores of length l_p and radius r_p. The pore dimensions range from a microscale of the order of Ångstroms to a macroscale which is a significant fraction of the particle radius. The radius of the largest pore is denoted by r_{max} and is given by

$$r_{max} = 2a\,\theta^{1/3}/3K_o \tag{1}$$

where θ is the total porosity of the particle and K_o is a constant of integration, approximately equal to five, which relates the pore length to its radius

$$l_p = K_o\, r_p/\theta^{1/3} \tag{2}$$

The radius of the smallest pore is denoted by r_{min} and is given by

$$r_{min} = 2\theta/\beta\,\rho_s s_p \tag{3}$$

where ρ_s is the density of the solid matrix, s_p is the specific internal surface area (several hundred m^2/g), and

$$\beta = \ln(r_{max}/r_{min}) \tag{4}$$

The particle contains a continuous distribution of pore sizes from r_{min} to r_{max} . The number of pores within an arbitrary plane of cross-sectional area A and with radius between r_p and $r_p + dr_p$ is denoted by $\bar{g}(r_p)A\,dr_p$. The pore distribution function $\bar{g}(r_p)$ is given by

$$\bar{g}(r_p) = \theta/2\pi\beta r_p^3 \tag{5}$$

where $\bar{g}(r_p)$ indicates an average over all inclination angles between the axis of the pore and the normal to the plane. Due to the random orientation of the pores, the intersection of a circular cylinder with a plane is an ellipse of average area $2\pi r_p^2$. Hence, the porosity is the $2\pi r_p^2$ moment of $\bar{g}(r_p)$ and the internal surface area is the $4\pi r_p$ moment of $\bar{g}(r_p)$. The expression for $\bar{g}(r_p)$ was derived (Simons and Finson,1979) from statistical arguments and has been validated through extensive comparison of the predicted volume and surface area distributions with mercury intrusion data (Stacy and Walker, 1972). This has been accomplished for coal, char derived from that coal (Kothandaraman et.al., 1984), sorbents, catalysts and even kidney stones from both men (low porosity oxalate) and women (high porosity phosphate).

A characteristic feature of the $1/r_p^3$ distribution depicts that the pore volume between r_{min} and r_p increases linearly with the natural log of r_p. It is the functional form of this relationship,

$$Pore\ Volume \propto \int_{r_{min}}^{r_p} r_p^2\, \bar{g}(r_p)\, dr_p \propto \ln r_p \tag{6}$$

that depicts the inverse cubic dependence of $\bar{g}(r_p)$ on r_p. A linear display of mercury intrusion volume vs. $\ln(r_p)$ always infers a $1/r_p^3$ distribution.

The number of pores within the bulk volume V whose pore radius is between r_p and $r_p + dr_p$ may be defined by $Vf(r_p)\,dr_p$. The pore volume is expressed as the $\pi r_p^2 l_p$ moment of $f(r_p)$ and the internal surface area is the $2\pi r_p l_p$ moment of $f(r_p)$. The pore size distribution functions ($f(r_p)$ and $\bar{g}(r_p)$) are clearly not independent. The definitions of porosity and internal surface area infer that $f(r_p)$ is related to $\bar{g}(r_p)$ by

$$\bar{g}(r_p) = f(r_p)\, l_p / 2 \tag{7}$$

Equation (7) simply states that the probable number of pores intersecting an arbitrary plane increases with the length of the pore and with the density of pores.

The length of a pore is determined by an arbitrary intersection with another pore and is expressed (Simons and Finson, 1979) as a collision integral over the pore distribution functions. The analysis suggests that l_p , $\bar{g}(r_p)$ and $f(r_p)$ are proportional to r_p , $1/r_p^3$ and $1/r_p^4$ respectively. The constants of proportionality are obtained from integral constraints, i.e., the total porosity and internal surface area contained in the pore structure. The expression for $f(r_p)$ is given by

$$f(r_p) = \frac{\theta^{4/3}}{\pi\, \beta\, K_o\, r_p^4} \tag{8}$$

where the constants were defined above.

The pore volume distribution corresponding to these distribution functions is similar to that utilized in the random pore model (Gavalas, 1980 & 1981). However, the pore tree model and the random pore model differ dramatically in their choice of the pore aspect ratio (length to diameter) and its implications with respect to pore branching. The random pore model allows a single pore to connect two larger pores. This picture lends itself to the idealization of instantaneous mixing between the pores and requires that the pore aspect ratio be of the order of one hundred. The pore tree theory uses data for r_{max} to imply (via K_o) that

all pores possess an aspect ratio of the order of ten. Hence, small pores may connect to larger pores only on one end and all pores must branch from successively larger pores like a tree or river system.

Each pore that reaches the exterior surface of the particle is depicted as the trunk of a tree. The size distribution of tree trunks on the exterior surface of the particle is denoted by $\bar{g}(r_t)4\pi a^2 dr_t$ where $\bar{g}(r_t)$ is functionally identical to $\bar{g}(r_p)$. Each trunk of radius r_t is associated with a specific tree-like structure. Let N_t be defined as the branch distribution function where $N_t dr_p$ is the number of pores of radius r_p (within size range dr_p) in a tree whose trunk radius is r_t . The total number of pores of radius r_p in a sphere of radius a may be expressed as $4/3\pi a^3 f(r_p)dr_p$ or, as the sum of all pores of radius r_p contained within every tree in the porous sample, plus all pores of radius r_p that are themselves the trunk of a tree. Hence,

$$\frac{4}{3}\pi a^3 f(r_p) = \int_{r_p}^{r_{max}} N_t \bar{g}(r_t) 4\pi a^2 dr_t + 4\pi a^2 \bar{g}(r_p) \tag{9}$$

where $\bar{g}(r_t)$ is the number of tree trunks per unit external area of the porous sample and only those trees whose trunk radius is greater than r_p may contain a pore of radius r_p. Using the previously derived expressions for r_{max}, $\bar{g}(r_p)$ and $f(r_p)$, Eq.(9) is identically satisfied by

$$N_t = r_t^3 / r_p^4 \tag{10}$$

The branch distribution function completely characterizes the pore tree. The internal surface area and pore volume associated with each pore tree are denoted by $S_t(r_t)$ and $V_t(r_t)$, respectively, and are expressed as the sum of the contributions from the trunk and that from the branches.

$$S_t(r_t) = 2\pi r_t l_t + \int_{r_{min}}^{r_t} 2\pi r_p l_p N_t dr_p \tag{11}$$

$$V_t(r_t) = \pi r_t^2 l_t + \int_{r_{min}}^{r_t} \pi r_p^2 l_p N_t dr_p \tag{12}$$

Using Eq.(10) for N_t, $S_t(r_t)$ and $V_t(r_t)$ become

$$S_t(r_t) = 2\pi r_t l_t \left(\frac{r_t}{r_{\min}}\right)(1-\theta) \tag{13}$$

$$V_t(r_t) = \pi r_t^2 l_t \left(1+\ln\left(\frac{r_t}{r_{\min}}\right)\right) \tag{14}$$

where the $(1-\theta)$ term in S_t has been included to account for pore combination (Simons, 1979).

The surface area associated with the pore tree may be several orders of magnitude greater than the surface area of the trunk. However, the volume of the pore tree may, at most, be one order of magnitude greater than that of the trunk. It should also be noted that the above expressions for S_t and V_t reduce to those appropriate to a single cylindrical pore in the limit of $r_t \rightarrow r_{min}$ (the leaf of the tree). Furthermore, the integrals of $S_t(r_t)$ and $V_t(r_t)$ over all $\bar{g}(r_t)$ recover the total internal surface area and pore volume of the porous sample.

Each trunk of radius r_t is associated with a specific tree-like structure with continuous branching to ever decreasing pore radii. The radius and number of pores is a unique function of the distance x into the tree. The coordinate x is skewed in that it follows a tortuous path through the branches of the tree. Let n(x) represent the number of pores of radius r_p at location x in a tree of trunk radius r_t. An analysis (Simons,1982) of this pore tree has demonstrated that

$$n(x) = r_t^2 / r_p^2(x) \tag{15}$$

and the coordinate x is related to r_p by

$$dr_p/dx = -r_p / l_t \tag{16}$$

The continuous branching model has been used to successfully describe char oxidation (Lewis and Simons, 1979; Simons, 1982 & 1983a), coal pyrolysis (Simons, 1983b & 1984) and the catalytic cracking of benzene by porous iron oxides (Simons et al., 1986). It was also used to successfully describe sulfur sorption (SO_2 and H_2S) by porous calcine (CaO) in the limit of zero utilization (Simons and Rawlins, 1980; Simons et al., 1984) and was later extended to include $CaSO_4$ and CaS deposits (Simons and Garman, 1986; Simons et al., 1987; Simons, 1988; Simons et al., 1988). The subsequent determination of the controlling physical parameters led to a new concept for the optimization of the sulfur sorption process (Simons, 1991; Simons et al., 1992) through spray drying of water soluble organic calcium solutions to control the sorbent pore structure.

III. INTERCONNECTIVITY

The first step in determining the size distribution of the interconnected pores and the distribution of the permeability is to determine the distribution function $\bar{G}_t(r_t, r_p)dr_p$ which represents the number of pores of radius r_p (within size range dr_p) per unit cross section of an arbitrary plane and also contained within a tree whose trunk radius is r_t. Consider an infinite homogeneous isotropic porous media and isolate a spherical volume of that media denoted by the radius a. Such a volume is illustrated in Fig. 2. The total number of pores of radius r_p (within size range dr_p) intersecting plane AA of area πa^2 has previously been defined by $\bar{g}(r_p)\pi a^2 dr_p$. The pores in plane AA in this size range may also be determined by integrating $\bar{G}_t(r_t, r_p)\pi a^2 dr_p$ over all trees whose trunk intersects the exterior surface of the porous sample. Hence it follows that

$$\bar{g}(r_p)\pi a^2 dr_p = \int_{r_p}^{r_{max}} [\bar{G}_t(r_t, r_p)\pi a^2 dr_p]\ \bar{g}(r_t)\, 4\pi a^2 dr_t \tag{17}$$

where only those trees whose trunk radius is greater than r_p may contain a pore of radius r_p.

A solution to Eq. (17) for $\bar{G}_t(r_t, r_p)$ will not necessarily be unique. Physical arguments will help determine $\bar{G}_t(r_t, r_p)$ and help ensure that it is the particular solution we seek. Since N_t represents the number of pores of size r_p in the tree and the probability of a pore intersecting a plane is proportional to its length, it follows that $\bar{G}_t(r_t, r_p)$ should be

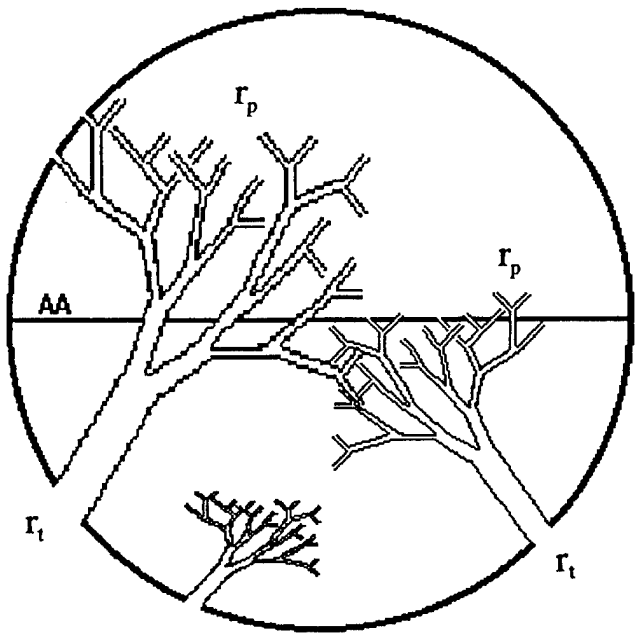

Figure 2. Spherical Volume of a Porous Media

proportional to the product of N_t and l_p/l_t , i.e., proportional to r_t^2/r_p^3. Eq. (17) is identically satisfied by a function which differs from r_t^2/r_p^3 by $\ln(r_p)$.

$$\bar{G}_t(r_t, r_p) = \frac{r_t^2}{4\pi a^2 r_p^3 \ln(r_{max}/r_p)} \tag{18}$$

Note that $\ln(r_p/r_{max})$ introduces an integrable singularity at $r_p=r_{max}$ such that $\bar{G}_t(r_t, r_p)\, dr_p$ is finite at $r_p=r_{max}$. Hence, there is one and only one largest pore for each reference sphere.

The probability of trees sharing common branches, i.e., the interconnectivity of the pore structure is described in Fig. 3. We seek the distribution function $\bar{I}(r_p)\, dr_p$ which represents the number of pores (within size range dr_p about r_p) per unit area of plane AA that are connected to both sides of the pore structure through pores at least as large as r_p. A_θ is defined as the area within plane AA that is **open to one side** of the porous media through all trees of size r_t' (through all pores of size r_p' that are at least as large as r_p). Subsequently, $A_\theta\, \bar{G}_t(r_t, r_p) dr_p$ represents the number of pores of size r_p (within size range dr_p) per unit area of plane AA that are contained in a tree of size range dr_t about r_t **and are also connected to the opposite side of the porous media** through all trees denoted by r_t'. It follows that the distribution function for interconnected pores in plane AA may be obtained by integrating $A_\theta\, \bar{G}_t(r_t, r_p) dr_p$ over all trees (r_t) that are large enough to contain a pore of size r_p . Hence,

$$\bar{I}(r_p)\pi a^2 dr_p = \int_{r_p}^{r_{max}} [A_\theta\, \bar{G}_t(r_t, r_p)\, dr_p]\, \bar{g}(r_t) 2\pi a^2 dr_t \tag{19}$$

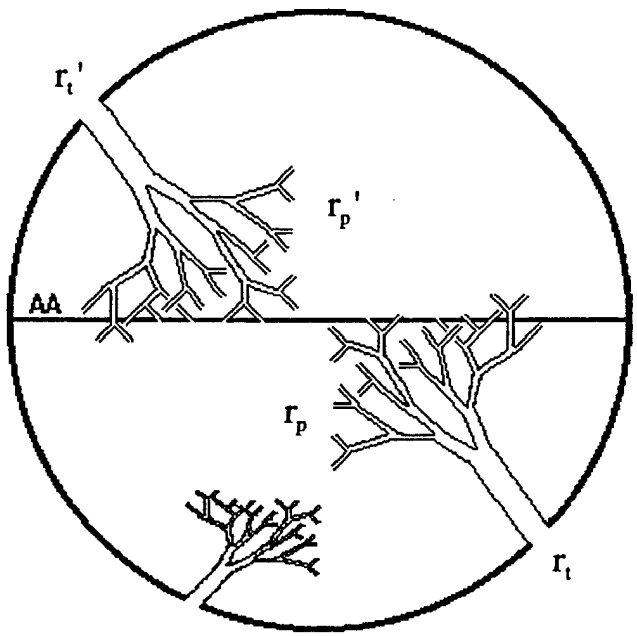

Figure 3. Interconnectivity of a Porous Media

From the above definition of A_θ , A_θ may be expressed as

$$A_\theta = \int_{r_p}^{r_{max}} [\int_{r_p}^{r_t} 2\pi r_p^2 \, \pi a^2 \bar{G}_t(r_t, r_p) \, dr_p] \, \bar{g}(r_t) \, 2\pi a^2 \, dr_t \tag{20}$$

where the primes on the variables of integration have been omitted. Evaluating Eq. (20) yields

$$A_\theta = \frac{\pi a^2 \theta \ln(r_{max}/r_p)}{2\beta} \tag{21}$$

from which Eq. (19) yields the common branch distribution function.

$$\bar{I}(r_p) = \frac{\theta \ln(r_{max}/r_p)}{4\beta} \, \bar{g}(r_p) \tag{22}$$

It has been deduced that the total number of common branches of size r_p in an arbitrary plane scales approximately with the total number of pores of that size in that plane. Hence, there is a probability of interconnectivity at pore size r_p that is logarithmic in pore size. Defining this probability as $P_I(r_p)$ via Eq. (22),

$$P_I(r_p) = \frac{\theta \ln(r_{max}/r_p)}{4\beta} \tag{23}$$

it is apparent that approximately one percent of all pores of all sizes are interconnected through larger pores.

The broad size range associated with the interconnectivity suggests that a very wide range of pore sizes control transport and that a complicated mixture of convective and diffusive transport persists through all of pore space. While permeability is dominated by the largest pores, it is important to determine the level of convection that is occurring in smaller pores in order to accurately describe the fine scale transport necessary to assess chemical reactions. In the following sections, bulk permeability, bulk diffusivity and small scale convection are addressed using the interconnectivity derived above.

IV. PERMEABILITY

The fundamental relationship governing convection in a porous media is Darcy's Law which relates the volume flow rate $\dot{Q}_p$ to the pore radius r_p and the pressure gradient $\frac{dP}{dx}$

$$\dot{Q}_p = \frac{\pi r_p^4}{8\mu}\left(-\frac{dP}{dx}\right) \tag{24}$$

where μ is the viscosity of the fluid. The bulk permeability (k) is defined in terms of the volume flow rate across the cross sectional area A

$$k = \frac{\dot{Q}\mu}{A(-dp/dx)} \tag{25}$$

Convection across plane AA in Fig. 4 will possess contributions from two primary sources illustrated in Figs. 4a and 4b. Fig. 4a illustrates the case where the convection in plane AA is due solely to the pores that are interconnected in that plane. Fig. 4b illustrates the case where the convection in plane AA is due to the smaller pores in the pore tree that are interconnected outside of plane AA. This connectivity will translate into a slower velocity in the pore crossing plane AA but could be significant because 99% of the pores in plane AA are not interconnected in that plane.

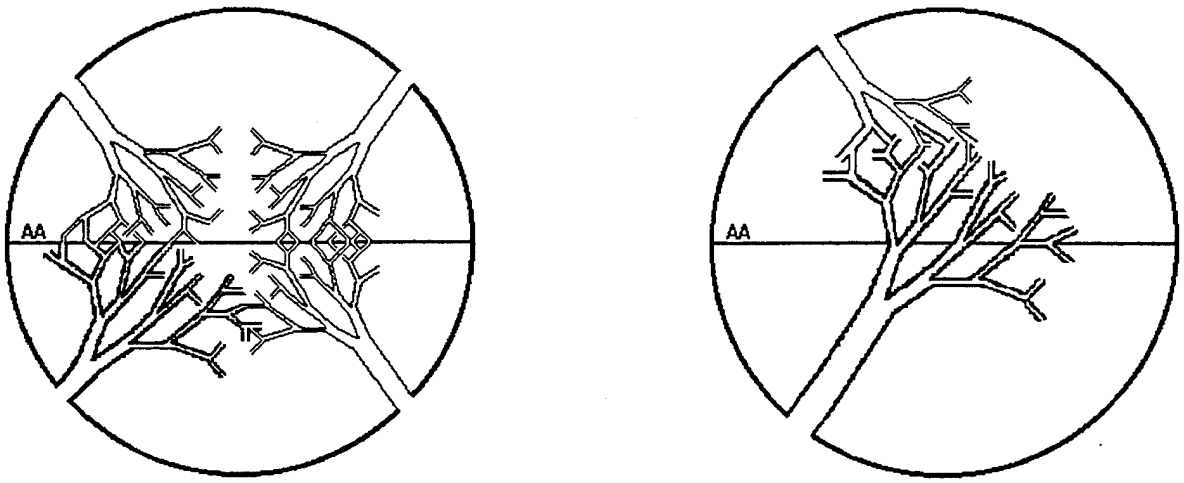

a) Pores Interconnected in Plane AA

b) Pores Interconnected Out of Plane AA

Fig. 4 Convection in the Pore Tree

Consider any pore of radius r_s in plane AA of Fig. 4b to be the trunk of a tree. Each pore of size r_p within the tree possesses the probability $P_I(r_p)$ of being interconnected and each interconnected pore in the tree will carry volume flow rate $\dot{Q}_p(r_p)$. Since there are $N_s dr_p$ (Eq. 10: $N_s = r_s^3/r_p^4$) pores in size range dr_p within the tree, the total volume flow rate $\dot{Q}_\infty(r_s)$ through trunk r_s in plane AA becomes

$$\dot{Q}_\infty(r_s) = \int_{r_{min}}^{r_s} \dot{Q}_p(r_p)\ P_I(r_p)\ N_s\ dr_p \tag{26}$$

or, to first order,

$$\dot{Q}_\infty(r_s) = \frac{\theta \pi r_s^4 \ln(r_{max}/r_s)}{32\,\mu\,\beta}\left(-\frac{dp}{dx}\right) + H.O.T \tag{27}$$

Within this approximation, it is seen that $\dot{Q}_\infty(r_s)$ is identical to the volume flowing through the pores that are interconnected within plane AA. i.e.,

$$\dot{Q}_\infty(r_s) \equiv \dot{Q}_p(r_s)\ P_I(r_s) \tag{28}$$

which demonstrates that all volume flow through plane AA in pore size r_s is dominated by the interconnectivity of size r_s in plane AA and not by the interconnectivity of smaller pores in subsequent branches of the pore tree. Simply stated: case 4a dominates case 4b.

Since all volume flow through plane AA is limited by the interconnectivity of the pores in that plane, Eq. (24) for the volume flow rate may be rewritten to include all interconnected pores in area A. Hence,

$$\dot{Q} = \frac{\pi A}{8\,\mu}\left(-\frac{dP}{dx}\right)\int_{r_{min}}^{r_{max}} r_p^4\ \bar{I}(r_p)\,dr_p \tag{29}$$

where $\bar{I}(r_p)$ is the "common branch distribution function" given by Eq. (22). The bulk permeability (k) is then expressed as

$$k = \frac{\pi}{8}\int_{r_{min}}^{r_{max}} r_p^4\ \bar{I}(r_p)\,dr_p \tag{30}$$

Upon integration, Eq. (30) becomes

$$k = \left(\frac{\theta r_{max}}{16 \beta} \right)^2 \tag{31}$$

Equation (31) resembles a dozen other expressions available in the literature wherein it is concurred that the bulk permeability is dominated by the largest pores in the media but the unknown value of that permeability is simply replaced by an unknown pore size to the second power. Since the pore size distribution function will be least accurate at the extreme end of the size range, i.e. at r_{max} , no claim can possibly be made that the numerical constants in Eq. (31) are in any way superior to those derived elsewhere. One important advantage of the extended pore tree model is that it characterizes the distribution of permeability in pore space, a feature that will be important in describing fine scale contaminant transport and in-situ remediation. A second advantage is the ability to assess statistical errors in the measurement of the permeability as a function of the measurement scale size. This exercise is also a good test of the extended pore tree model.

Consider a soil sample with the following physical characteristics:

Conductivity:	v =2 cm/hr
Permeability:	k =0.6 Darcy
Porosity:	θ =50%
Pore Aspect Ratio:	K_o=5
$\ln(r_{max}/r_{min})$	β =12

From Eq. (31), it follows that

$$r_{max} = 300 \ \mu m$$

and subsequently r_{min} = 20 Å. The size of the smallest pore is not an important parameter for this application but may be readily adjusted through a minor variation in the value of β (e.g., for r_{min} of the order of 100 Å, β = 10). The bold assertion made in applying this pore structure model to soil is that the $1/r_p^3$ pore size distribution is valid between r_{min} and r_{max}.

To investigate the role of the measurement scale size on permeability, consider the largest pore r_{max} contained in the spherical sample of radius "a" as given by Eq. (1). Since r_{max} in Eq. (31) for the permeability represents the largest pore in the media, the corresponding value of "a" is denoted a_{max} and represents the largest sample size for which the pore sizes will scale with the dimensions of the sample. From Eqs. (1) and (31)

$$a_{max} = \frac{24 K_o \beta}{\theta^{4/3}} \sqrt{k} \tag{32}$$

Each sphere of radius a_{max} will contain <u>one</u> pore of size r_{max}. A 20 x 20 grid of these spheres

will be characterized by the dimension $40a_{max}$ and contain 400 pores of size r_{max}. Each of these pores possess probability $P_I(r_p)$ of being interconnected. Following Eq. (23), $P_I(r_p)$ is approximately 0.0025 for r_p sufficiently close to r_{max}. Hence, only <u>one</u> of the 400 largest pores in this 20 x 20 grid will be interconnected and the error in the measurement of the permeability will correspond to the statistical error of 100% associated with that of a sample number of unity. Carrying this argument to a 200 x 200 grid of dimension $400a_{max}$, there will be 100 interconnected pores corresponding to a statistical error of 10%. Similarly, a grid of scale $4000a_{max}$ will reduce the error to 1%.

Figure 5 illustrates the predicted permeability measurement error associated with the soil sample characterized above (a_{max} =0.3 cm). Note that the errors associated with the measurement of permeability become negligible as the measurement scale size approaches several meters. This has been confirmed by the infiltration data of Shouse et. al. (1994). The measured value of hydraulic conductivity asymptotes to 2 cm/hr at measurement scales greater than 4 meters. At smaller measurement scales, the inferred measurement error is calculated under the assumption that the asymptote is precisely 2 cm/hr. The excellent agreement between the predicted and inferred error supports the extension of the pore tree model to describe a porous permeable media.

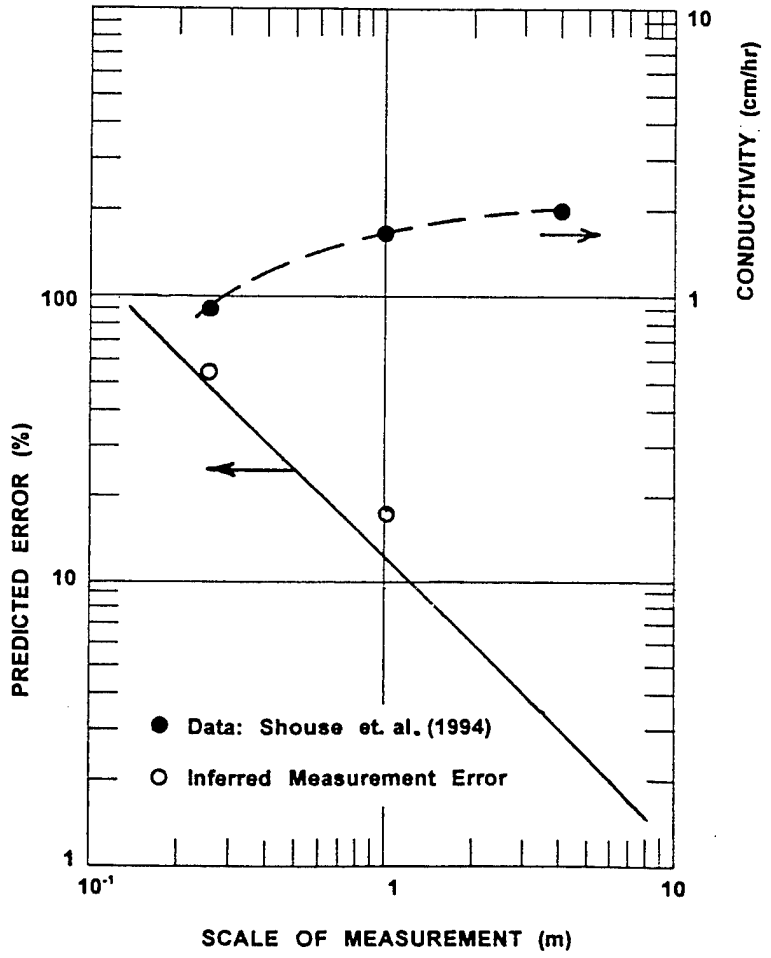

Figure 5. Error in Permeability Associated with the Measurement Scale

V. BULK GASEOUS DIFFUSION IN A PARTIALLY SATURATED MEDIA

The extended pore tree model is readily adapted to a partially saturated media through the assumption that all of the water is contained in pore sizes between r_{min} and r_{sat} while only gas is contained between r_{sat} and r_{max}. Since, by Eq. (6), porosity is distributed as $\ln(r_p)$ in pore space, the porosity associated with the air filled pores (θ_a) is approximated by

$$\theta_a = \frac{\ln(r_{max}/r_{sat})}{\beta}\,\theta \tag{33}$$

where r_{sat} is treated as an independent variable of the saturated pore structure. No gaseous diffusion is allowed within $r_p \le r_{sat}$. With this restriction, the extended pore tree model is used to develop an explicit relationship between bulk gaseous diffusivity and the permeability which is validated through the diffusivity data of Washington et. al., (1994). It is demonstrated that the gas diffusivity scales as $1/r_{sat}$ and it is the sensitivity of r_{sat} to the saturated volume that controls the saturated diffusivity.

The diffusive mass flux in a single pore is given by

$$\dot{M}_p(r_p) = \pi\, D_g\, r_p^2 \left(\frac{-\partial \rho_c}{\partial x}\right) \tag{34}$$

where D_g is the continuum gas diffusion coefficient (D_g=0.2 cm^2/s). Continuum gas phase diffusion is valid only for pore radii sufficiently large that D_g is greater than the Knudsen diffusion coefficient, $D_{Kn}=2Vr_p/3$, where V is the mean thermal speed of a molecule. Knudsen diffusion is characterized by gas collisions with the pore walls and is valid only for $r_p \le 3D_g/2V = 0.1\mu m$. The limit of validity of Eq. (34) is denoted by r^*_{sat}, the larger of either r_{sat} or $3D_g/2V$. This limit restricts continuum gaseous diffusion from both the saturated pores and the unsaturated pores controlled by free molecule flow.

Just as in the case of convection, it must be determined whether the mass flux across plane AA in Fig. 4 is determined by the interconnectivity of the smaller pores out of the plane (Fig. 4b) or by only those pores that are interconnected in the plane (Fig. 4a). Consider any pore of radius r_s in plane AA of Fig. 4b to be the trunk of a tree. Each pore of size r_p within the tree possesses the probability $P_I(r_p)$ of being interconnected and each interconnected pore in the tree will carry the mass flow rate $\dot{M}_p(r_p)$. Since there are $N_s dr_p$ (Eq. 10: $N_s=r_s^3/r_p^4$) pores in size range dr_p within the tree, the total mass flow rate $\dot{M}_\infty(r_s)$ through each and every trunk of radius r_s in plane AA becomes

$$\dot{M}_\infty(r_s) = \int_{r^*_{sat}}^{r_s} \dot{M}_p(r_p)\, P_I(r_p)\, N_s\, dr_p \tag{35}$$

Integration of Eq. (35) yields the mass flux (case 4b) for each trunk of radius r_s

$$\dot{M}_{\infty}(r_s) = \frac{\pi D_g \theta_a r_s^3}{4 r_{sat}^*} \left(\frac{-\partial \rho_c}{\partial x} \right) \tag{36}$$

where a $\ln(r_{max}/r_{sat})$ term was eliminated via Eq. (33).

If the mass flux through plane AA is limited by the pores that are interconnected in that plane (case 4a), the mass flux is expressed as $\dot{M}_p(r_s) P_I(r_s)$, and it is immediately seen that

$$\dot{M}_{\infty}(r_s) \gg \dot{M}_p(r_s) P_I(r_s) \tag{37}$$

i.e., case 4b dominates case 4a. Since the mass diffusion in plane AA is determined by the pore interconnectivity of the smaller pores outside of plane AA, the saturation of those smaller pores becomes an important element in the bulk gaseous diffusion.

Since each pore of radius r_s in plane AA carries mass flux $\dot{M}_{\infty}(r_s)$, the bulk diffusion coefficient is obtained by integrating Eq. (36) over all pores in that plane

$$D_{bulk} = \int_{r_{sat}^*}^{r_{max}} \frac{\pi D_g \theta_a r_s^3}{4 r_{sat}^*} \bar{g}(r_s) dr_s \tag{38}$$

or, upon integration

$$D_{bulk} = \frac{D_g \theta \theta_a r_{max}}{8 \beta r_{sat}^*} \tag{39}$$

and upon eliminating r_{max} via Eq. (31), the bulk diffusivity D_{bulk} is expressed in terms of the permeability k.

$$D_{bulk} = \frac{2 D_g \theta_a \sqrt{k}}{r_{sat}^*} \tag{40}$$

The bulk diffusivity cannot increase indefinitely with increasing permeability as inferred by Eq. (40). In deriving this expression, the mass flux through the interconnected branches of the tree was not constrained from exceeding the diffusive capabilities of the trunk

itself. To correct this potential problem, the limit of D_{bulk} is determined as the maximum diffusive flux in pore r_s integrated over all pores in plane AA.

$$D_{limit} = \int_{r_{min}}^{r_{max}} \pi D_g r_s^2 \, \bar{g}(r_s) dr_s = \frac{D_g \theta}{2} \tag{41}$$

This limit is illustrated in Figure 6 together with the predicted values of D_{bulk} for an extended range of values of permeability and the saturation radius, r_{sat}. Model predictions correspond to the measured values of θ_a=0.2 and θ=0.5 from Washington et. al., (1994), and the diffusivity data suggest a value of r_{sat} in the range of 10 μm to 100 μm. An exact comparison of the present theory to the least squared fit of the data suggests a value of 30 μm. While the excellent agreement with the data of Washington et. al., (1994) does substantiate the present theory, there is clearly a very wide range of possible values for D_{bulk} in partially saturated soil which will depend upon an unknown saturation radius. A two order of magnitude decrease in the saturation radius will increase the bulk diffusivity by two orders of magnitude and yet the corresponding increase in the air filled porosity is, by Eq. (33), only 33%. Hence, field measurements of the unsaturated volume are not sufficiently accurate to correlate bulk diffusivities. If bulk diffusivities are to be correlated with field data, such measurements should attempt to measure the saturation radius.

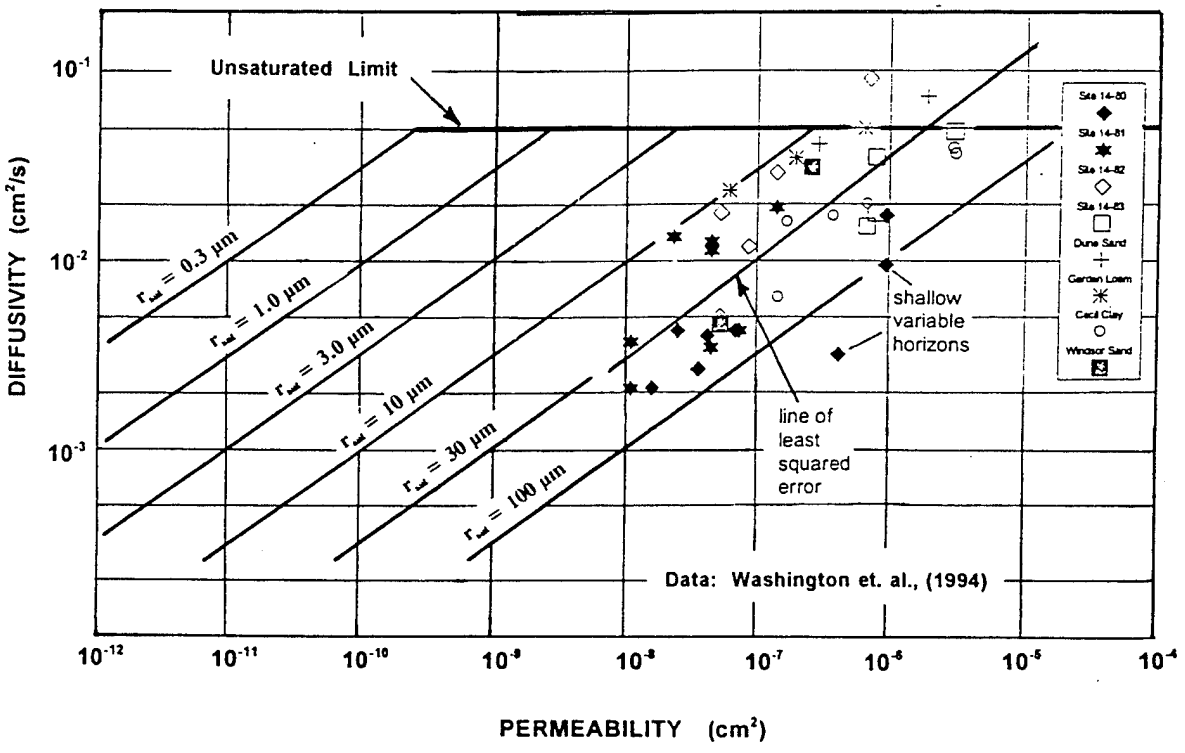

Figure 6. Bulk Diffusivity of a Partially Saturated Soil

VI. PERMEABLE SUB-RANGE

The present theory offers the opportunity to investigate some of the features of the pore structure that are relevant to the fine scale contaminant transport and remediation reactions. One such feature is the distribution of permeability in pore space. While the bulk permeability is dominated by the largest pores, some permeability occurs in smaller pores. It is the balance of the sub-scale convection with the small scale diffusion that will control contaminant transport and in-situ remediation.

The analysis and data comparison on the errors introduced by the measurement scale size, section IV, has shown that soil with a bulk permeability of 0.6 Darcy possesses, on average, one large interconnected pore in any 12 cm by 12 cm cross section. To allow the penetration of the permeate throughout such a coarse grid, it will be shown that there is a very extensive permeable sub-range in the pore structure which does not contribute significantly to the bulk permeability but in which convection dominates diffusion.

To evaluate the permeable sub-range, Eq. (31) is rewritten to express the permeability contained in pores of radius r_p ($r_p \le r_{max}$) or smaller

$$k_{sr} = \left(\frac{\theta r_p}{16 \beta} \right)^2 \tag{42}$$

where k_{sr} represents the permeability in the sub-range dimension to be defined by $L_{sr}(r_p)$. It was deduced above that $L_{sr}(r_p)$ must be selected such that there is at least one interconnected pore of radius r_p in cross-sectional area L_{sr}^2 in order for k_{sr} to be accurate to order unity. Subsequently, a 20 x 20 grid of spheres of radius a_{sr} will contain one interconnected pore of radius r_p

$$L_{sr}(r_p) = 40 a_{sr} \tag{43}$$

where a_{sr} is given by Eq. (32) with k replaced with k_{sr}.

$$a_{sr} = \frac{24 K_o \beta}{\theta^{4/3}} \sqrt{k_{sr}} \tag{44}$$

Eqs. (42) to (44) represent the scaling of the pore structure with scale size for all $r_p \le r_{max}$ or for all $a \le a_{max}$ and all $L_{sr}(r_p) \le L_{sr}(r_{max})$. The balance of convection and diffusion within these scale sizes may be assessed.

The convective flux of species "c" with mass density ρ_c across area L_{sr}^2 is denoted by

$$\dot{M}_k = \rho_c \dot{Q} = k_{sr} L_{sr}^2 \rho_c (-dp/dx)/\mu \tag{45}$$

and the diffusive mass flux across the same cross section is expressed as

$$\dot{M}_D = D_{eff}(\rho_c / L_{sr})\, L_{sr}^2 \tag{46}$$

where the characteristic gradient of ρ_c is ρ_c / L_{sr} and the effective diffusion coefficient is D_{eff}.

The balance between convection and diffusion occurs on the length scale L where the convective and diffusive mass fluxes are equal. From Eqs. (45) and (46)

$$L = 100\left(\frac{\mu D_{eff}\beta^2 K_o^2}{\theta^{8/3}(-dp/dx)}\right)^{1/3} \tag{47}$$

The boundary between convective and diffusive transport is illustrated in Figure 7 for a solute in a saturated porous media. The effective diffusion coefficient is assumed to be given by the porosity times the solute self diffusion coefficient D_s ($D_s \approx 10^{-5}$ cm^2/s). The boundary between

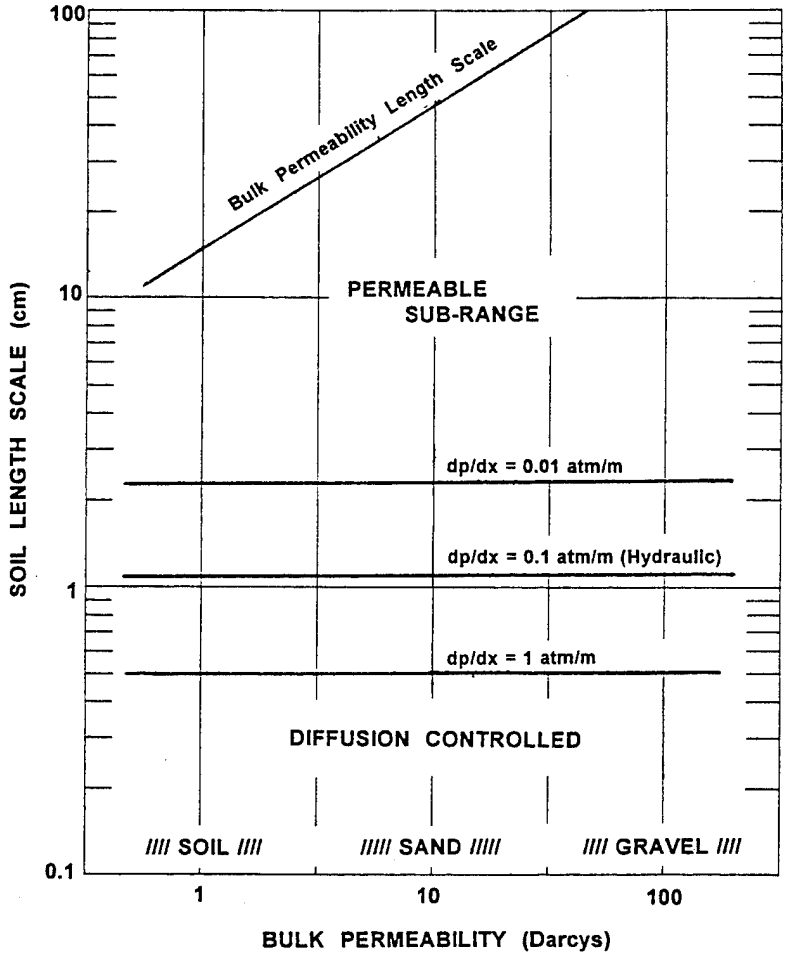

Figure 7. Permeable Sub-Range for Convection in a Saturated Porous Media

sub-scale convection and diffusion is illustrated for the solute in water (μ = 0.01 poise) at pressure gradients of 0.01 atm/m, 0.1 atm/m (hydraulic) and 10 atm/m. Also illustrated is the length scale associated with the spacing of the large pores controlling the bulk permeability (Eqs. (43) and (44) in the limit of $r_p \rightarrow r_{max}$). The results depict a very extensive permeable sub-range at bulk permeabilities characteristic of soil, sand and gravel. For soil with a bulk permeability of 1 Darcy, the large interconnected pores are nominally 15 cm apart. The soil matrix between the large pores experiences a convective mass flux through its smaller pores whose mass flow rates are much smaller than that of the bulk permeability but greater than that possible by diffusion. At length scales of order one centimeter, diffusion becomes rate limiting. Hence, this pore structure model provides a methodology for determining the length scale separating the mobile and immobile regions of the soil. The theory depicts that the size of the immobile region is primarily a function of the pressure gradient.

When the above analysis is applied to gas phase diffusion in an unsaturated media, μ is of the order of 10^{-4} poise and D_{eff} is 0.05 cm^2/s (Figure 6). The boundary between convection and diffusion occurs on length scales five times as large as those depicted in Figure 7 for the same pressure gradients. While the size of the permeable sub-range is severely reduced, the entire distribution of species "c" is still limited by a diffusive length scale that is primarily a function of the gas pressure gradient. Hence, the length scale separating the mobile and immobile regions of the soil is of the order of five centimeters at gas pressure gradients equal to the hydraulic pressure gradient (0.1 atm/m) and of the order of 10 cm at 0.01 atm/m.

Similarly, when the above analysis is applied to gas phase diffusion in a partially saturated media, μ is of order 10^{-4} poise and D_{eff} may be as low as 10^{-3} cm^2/s (Figure 6). Under these conditions, the boundary between convection and diffusion occurs at length scales identical to those depicted in Figure 7 and the existence of a permeable sub-range is preserved. However, for a partially saturated media, D_{bulk} should be used for D_{eff} . From Eq. (40) we write

$$D_{eff} = \frac{2 D_g \theta_a \sqrt{k_{sr}}}{r^*_{sat}} \tag{48}$$

from which it follows that the length scale separating the mobile and immobile regions of a partially saturated soil has a slightly stronger pressure gradient dependence

$$L = 44 \left(\frac{\mu \beta K_o D_g \theta_a}{\theta^{4/3} r^*_{sat} (-dp/dx)} \right)^{1/2} \tag{49}$$

It is anticipated that the concept of the permeable sub-range will help researchers develop relatively simple, physics based submodels for the ground water/remediation codes. If these submodels were tested independently from the codes, the codes themselves would not require parameter "fitting" and could become more directive than interactive.

VII. SUMMARY

The pore tree model has been extended to describe the permeable pore structure which characterizes the subsurface transport of gas and water in soil, the dispersion of contaminants, and the in-situ remediation of contaminated sites. The random nature of the pore structure, which formed the basis of the statistical derivation of the pore tree, is applied to porous soil and sand. The interconnectivity of the pore structure is obtained via a statistical determination of the "branches" that are common to several trees to allow convection and bulk diffusion through the large scale (mobile) structure in addition to diffusion and coupled chemical reactions within the smaller scale (immobile) structure. The statistical analysis reported above has determined that the probability of pore interconnectivity extends across the entire pore size range, with a slight increase in the probability accompanying a decreasing pore size. While permeability is dominated by the largest pores, it is also important to establish the level of convection and diffusion that is occurring at the intermediate scales in order to accurately relate large scale bulk transport, small scale diffusion and coupled chemical reactions.

The permeability across a given plane is limited by the largest pores that are interconnected in that plane. The statistical analysis has determined that approximately one quarter of one percent of all large pores are interconnected. This establishes a very coarse grid for the permeability which leads to measurement scale size errors. The extended pore tree model has successfully explained the measurement errors in the permeability of soil due to the measurement scale size (Shouse, et.al., 1994) which has indirectly confirmed the low probability of the interconnectivity.

The bulk gaseous diffusivity across a given plane is shown to be limited by the interconnectivity of the smaller branches outside of that plane. These small pores may be saturated, resulting in a strong dependence of the diffusivity on the radius of the saturated pore. A comparison of the present theory to the diffusivity data of Washington et. al., (1994) suggests a saturation radius of 30 μm. While the excellent agreement with the data does substantiate the present theory, the diffusivity in partially saturated soil is very sensitive to an unknown saturation radius. If bulk diffusivities are to be correlated with field data, such measurements should attempt to measure the saturation radius.

The permeability and the bulk diffusivity have tested two extreme limits of the pore structure and pore interconnectivity concepts. Permeability is limited by the in plane interconnectivity (Fig.4a) and bulk gaseous diffusion is limited by the out of plane (Fig. 4b) interconnectivity. Permeability is limited by the large pore interconnectivity and bulk diffusion is limited by the interconnectivity of the smaller pores. The apparent success of these concepts over a very broad pore size range suggests that the extended pore tree model will accurately describe the relationship between large scale convection and small scale diffusive transport.

Analysis of the permeability has utilized the interconnectivity of the pores to determine the distribution of the permeability with pore size. This analysis suggests the existence of a permeable sub-range in the pore structure which does not contribute significantly to the bulk permeability but in which convection dominates diffusion. It is the balance of the sub-scale convection with the small scale diffusion that will control contaminant transport and

in-situ remediation. Preliminary estimates suggest that the length scale separating the mobile and immobile regions of the soil is of the order of one cm. Smaller grains are, on a unit mass or size basis, more reactive than the larger grains. Hence smaller grains will locally deplete more nutrients or remediation chemicals from the convective flow than their larger counterparts. Simultaneously, the smaller pores surrounding the smaller grains offer more resistance to convection and a reduced amount of nutrients or remediation chemicals will be available in the convective flow. The size distribution of the pores and grains, and the variations in fluid velocity within and between pores of different sizes is critical to interfacing these transport processes. Future plans include the development of a methodology to couple convection and small scale diffusion upon which coupled chemical reactions may be added to accurately describe contaminant transport and in-situ remediation.

VIII. REFERENCES

Gavalas, G.R. (1980), "A Random Capillary Model with Application to Char Gasification at Chemically Controlled Rates," AIChE J., 26, 577.

Gavalas, G.R. (1981), "An Analysis of Char Combustion Including the Effect of Pore Enlargement," Comb. Sci. Tech., 24, 197.

Kothandaraman, G. and Simons, G.A. (1984), "Evolution of the Pore Structure in PSOC 140 Lignite During Pyrolysis," The Combustion Institute, Twentieth Symposium (International) on Combustion, Ann Arbor, MI.

Lewis, P.F. and Simons, G.A. (1979), "Char Gasification: Part II. Oxidation Results," Comb. Sci. Tech., 20, 3 & 4, 117-124.

Shouse, P.J., Ellsworth, T.R. and Jobes, J.A. (1994), "Steady-State Infiltration as a Function of Measurement Scale," Soil Science, 157, 3, 129-136.

Simons, G.A. and Finson, M.L. (1979), "The Structure of Coal Char: Part I. Pore Branching," Comb. Sci. Tech., 19, 5 & 6, 217-226.

Simons, G.A. (1979), "The Structure of Coal Char: Part II. Pore Combination," Comb. Sci. Tech., 19, 5 & 6, 227-235.

Simons, G.A. and Rawlins, W.T. (1980), "The Reaction of SO_2 and H_2S with Porous Calcined Limestone," Ind. & Eng. Chem., Process Des. & Dev., 19, 565-572.

Simons, G.A. (1982), "The Pore Tree Structure of Porous Char," The Combustion Institute, Nineteenth Symposium (International) on Combustion, Haifa, Israel.

Simons, G.A. (1983a), "The Role of Pore Structure In Coal Pyrolysis and Gasification," (Invited Survey Article) Progress in Energy and Combustion Science, 9, 269.

Simons, G.A. (1983b), "Coal Pyrolysis I. Pore Evolution Theory," Comb. and Flame, 53, 83-92.

Simons, G.A. (1984), "Coal Pyrolysis II. Species Transport Theory," Comb. and Flame, 55, 181-194.

Simons, G.A., Garman, A.R., and Boni, A.A. (1984), "High Pressure Sulfur Sorption by Limestone," Paper No. 33, Eastern Section of the Combustion Institute, Fall Technical Meeting, Clearwater Beach, FL.

Simons, G.A., Ham, D.O., and Moniz, G.A. (1986), "Catalytic Cracking of Aromatic Hydrocarbons", Physical Sciences Inc. PSI-385/TR-552, DOE/MC/21385-2021.

Simons, G.A. and Garman, A.R. (1986), "Small Pore Closure and the Deactivation of the Limestone Sulfation Reaction," AIChE J., 32, 1491.

Simons, G.A., Garman, A.R., and Boni, A.A. (1987), "The Kinetic Rate of SO_2 Sorption by CaO," AIChE J., 33, 211.

Simons, G.A. (1988), "Parameters Limiting Sulfation by CaO," AIChE J., 34, 167.

Simons, G.A., Parker, T.E., and Morency, J.R. (1988), "The Oxygen Reaction Order of SO_2 with CaO," Comb. & Flame, 74, 107.

Simons, G.A. (1991), "Predictions of CMA Utilization for In-Situ SO_2 Removal in Utility Boilers," International Symposium on Calcium Magnesium Acetate (CMA), Northeastern University, Boston, MA, May 14-16. Also: Resources, Conservation and Recycling, 7, 161-170, 1992.

Simons, G.A., Parker, T.E., Moore, J.W., Senior, C.A., and Levendis, Y.A. (1992), "Combined NO_x/SO_x Control Using a Single Liquid Injection System," Physical Sciences Inc., TR-1169.

Stacy,W.O. and Walker, Jr., P.L. (1972), "Structure and Properties of Various Coal Chars," Coal Research Section, College of Earth and Mineral Sciences, The Pennsylvania State University, PB 233996.

Washington, J.W.; Rose, A.W.; Ciolkosz, E.J.; and Dobos, R.R. (1994), "Gaseous Diffusion and Permeability in Four Soil Profiles in Central Pennsylvania," Soil Science, 157, 2, 65-76.